Electrical Power and Energy Systems 106 (2019) 33–44

Contents lists available at ScienceDirect

Electrical Power and Energy Systems

journal homepage: www.elsevier.com/locate/ijepes

Complementary power generation of double linear switched reluctance generators for wave power exploitation

J.F. Pan[a], Qianlong Li[a], Xiaoyu Wu[a], Norbert Cheung[b], Li Qiu[a,*]

[a] College of Mechatronics and Control Engineering, Shenzhen University, Shenzhen, Guangdong Province, China
[b] Department of Electrical Engineering, Hong Kong Polytechnic University, Hong Kong, China

ARTICLE INFO

Keywords:
Wave power
Linear switched reluctance generator
Finite element method

ABSTRACT

The wave power generation system based on the single linear generator scheme has low energy output and week robustness, especially in low speed conditions and parameter variations. To overcome the problem, a scheme of complementary power compensation generation for two asymmetric bilateral linear switched reluctance generators (ABLSRGs) is proposed in this paper. Mathematic model is first derived and machine characteristics are investigated by the finite element method. The compensation scheme is carefully investigated together with the independent control method. Under the conditions of parameter and velocity variations, experimentation demonstrates that both the voltage control accuracy and system robustness can be guaranteed with the proposed complementary power generation control scheme. Experiment results show that a voltage control precision of 11.75–12.23 V can be obtained, with the voltage reference of 12 V.

1. Introduction

The oceans possess enormous energy storage and an estimated wave power of more than 1 TW can be estimated [1]. The motions of waves can be ideally regarded as quasi-sinusoidal waveforms with the speed range normally falling into 0–2 m/s [2,3]. At present, wave power exploitation schemes are more and more focused on the direct-drive energy conversion methods [4–6]. By direct capture of translational wave energy in one dimensional, the linear generators can be employed to eliminate intermediate mechanical translators or converters from the traditional wave energy converters (WECs) that require linear-to-rotary power transformation mechanisms [7]. Therefore, the direct-drive WECs have the advantages of a simpler power take-off system with higher power efficiency [8]. Current research mainly concentrates on linear synchronous permanent magnetic generators (LSPMGs) [9], linear switched reluctance generators (LSRGs) and linear induction generators [10,11]. Though LSPMGs have relatively higher force-to-volume ratio and efficiency, the involvement of permanent magnets (PMs) often results in sophisticated assembly of PMs or winding schemes [12]. Therefore, the overall manufacture and assembly cost for such power generation systems based on LSPMGs are high. Moreover, the environment of wave power generation in the ocean experiences constant temperature variations and inevitably, this affects the normal operations of PMs [13] and the demagnetization of PMs will eventually cause performance deterioration or even malfunction of the entire power generation systems [14].

Like wind energy, the power density of wave is low for a designated ocean area. For any single direct-drive WECs, to keep power output at a reasonable level, the WECs should be designed with the dimensions comparable to five times of a standard human height [10]. However, for any single low-cost, low-power direct-drive WECs, the generator has low energy output and week robustness. Therefore, it is suggested that a certain number of linear WECs be deployed in a certain area and the deployed WECs extract the power coordinately in such area [15]. To keep the total generation cost at a reasonable price level, it is natural that the deployed linear WECs should have simple mechanical structures and they should be suitable for mass production as well [16]. LSRGs do not involve any PMs and the machines only consist of silicon-steel sheets, aluminum and copper wires. LSRGs have the characteristics of simple and robust mechanical structures and they are more suitable for the operation under the hostile environment. Though the efficiency is comparatively low, compared to their LSPMG counterparts, LSRGs are superior for the deployment of wave power generation in large numbers, since the manufacture and assembly cost is reasonable and the LSRGs are more suitable for mass production [17].

For single linear generator based power generation systems, current research mainly focuses on current commutation optimization and regulation, voltage and power control algorithms. In [18], a rectangular

* Corresponding author at: Postal Code: 518060, S604, Fundamental Laboratory Building Phase II, Southern Campus of Shenzhen University, Shenzhen, China.
E-mail address: qiuli@szu.edu.cn (L. Qiu).

https://doi.org/10.1016/j.ijepes.2018.09.023
Received 7 July 2017; Received in revised form 15 August 2018; Accepted 13 September 2018
Available online 01 October 2018

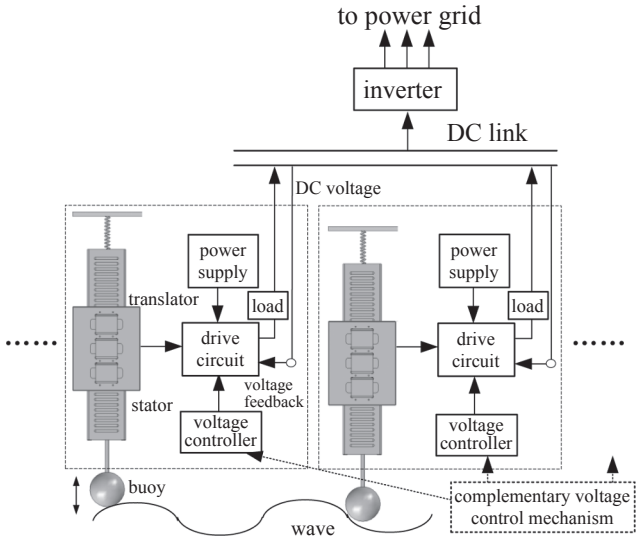

Fig. 1. Concept of complementary power generation.

current commutation scheme is proposed for the free-piston linear generator. A single switch chopping scheme for the output power control and the double switches chopping scheme for the phase current control are discussed for the LSRG, based on simulation [19]. Both open loop with turn-on and turn-off position optimization and closed loop current regulation scheme are investigated for the sensorless LSRG [8]. In [16], the closed loop current control scheme based on pulse width modulation is proposed. A DC link voltage control scheme is proposed to attenuate the low frequency ripple of a LSPMG [20]. In [10], the authors adopt a dual-loop control scheme to improve the voltage output precision with an optimized current distribution function. Power control is applied by directly collecting the power from individual coils for a linear, direct drive, air-cored, tubular, permanent magnet generator [21].

To realize coordinated power generation for multiple LSRGs, this paper first attempts to investigate the complementary power generation of two asymmetric bilateral LSRGs (ABLSRGs). Since the characteristics of the phase current are direct current (DC) pulsed waveforms [14], it is important to keep the quality of the output DC voltage signal at a reasonable level for future inversion or even grid connection.

The wave power generation system based on multiple LSRGs can be found in Fig. 1. As the buoys travel with waves, the translators are propelled and move along with the buoys. According to the working principle of LSRGs, current from each phase of the LSRGs can be generated based on the proper phase excitation scheme according to position. The load regulates the phase current from each phase to DC voltage. By the regulation of voltage control schemes, DC voltage signals can be output from the drive circuits to the DC link. Then the DC voltage can be inverted to three-phase alternating current (AC) for grid connection. More linear generators can be included in the power generation system for the contribution to the DC link. If each generator outputs the voltage to the DC link individually, it is called the "independent power generation" scheme. Since each generator generates power alone and neglects the wave energy input from others, in this scheme, the quality of the voltage from the DC link cannot be guaranteed. Since voltage ripples influence the inverted AC signals, it is important to keep the ripples at a reasonable level to facilitate the future applications for grid connection.

Instead of independent power generation, the two linear generators can work complementarily to achieve the ultimate goal of output voltage precision and increase the power volume at the same time. With the introduction of the complementary voltage control mechanism in Fig. 1, the two linear generators can work cooperatively to improve the precision of the total voltage from the DC link.

The innovation of this paper can be summarized as follows. First, the investigation of two identical ABLSRGs for wave power generation is investigated. Second, an effective voltage complementary scheme is proposed, based on theoretical analysis. Third, experimental results for performance comparisons under the independent and complementary control of ABLSRGs are carried out. Experimental results prove that the proposed power complementary control scheme not only ensures output voltage precision, but owns certain robustness under the conditions of control parameters or speed variations. An absolute output voltage value of 11.75–12.23 V can be achieved with 12 V voltage reference under the environment of parameter change or speed variations.

2. The ABLSRG and characteristics

The magnetic structure and picture of the ABLSRGs can be found in Fig. 2(a) and (b). The linear generator mainly consists of a stator base with stator blocks. The generator utilizes an asymmetric machine structure. Instead of perfect mirroring along the axis of the moving platform, both the stator and the mover phases apply an asymmetric scheme to improve a higher force-to-volume ratio and efficiency [17]. The moving platform is supported by a pair of linear guides. Each phase of the ABLSRGs has the same dimensions and ratings and the phases are defined as AA′, BB′ and CC′, respectively. Major specifications can be found in Table 1.

3. Theoretical background and characteristics

The ABLSRG can be considered as a typical energy transformation system and the motion equation can be described as [22],

$$F_j = M\frac{d^2x_j}{dt^2} + Q\frac{dx_j}{dt} + f_j \quad (j = 1, 2) \tag{1}$$

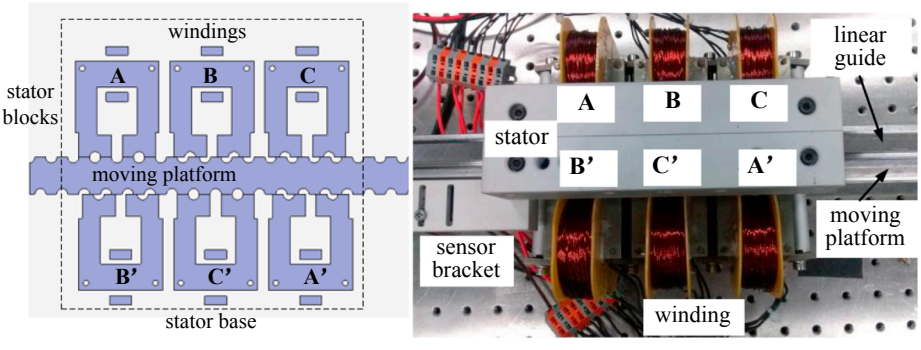

(a) (b)

Fig. 2. The LSRM (a) and machine structure (b).

Table 1
Major machine specifications.

Parameter	Value
Rated power	250 W
Pole width	6 mm
Pole pitch	6 mm
Phase resistance	2 ohm
Stack length	200 mm
Stroke length	350 mm
Air gap length (g)	0.3 mm
Number of turns	220

where F_j is the mechanical force input, M is the mass of the mover track, Q is the friction coefficient, f_j stands for the electromagnetic force and x_j is the position of the mover for the j-th generator. From the electrical terminal, any ABLSRG can be described in the form of the voltage balance equation as [23],

$$u_{j_k} = R_{j_k} i_{j_k} + \frac{d\lambda_{j_k}}{dt} \quad (k = AA', BB', CC') \tag{2}$$

with $\lambda_{j_k} = L_{j_k} i_{j_k}$, where u_{j_k} and λ_{j_k} stand for the voltage drop and flux-linkage of the k-th winding for the j-th generator, respectively. i_{j_k}, R_{j_k} and L_{j_k} are the phase current, resistance and inductance of the j-th generator, (2) can be further represented as the inductance form as [8],

$$u_{j_k} = R_{j_k} i_{j_k} + \left[\frac{\partial L_{j_k}}{\partial i_{j_k}} i_{j_k} + L_{j_k}\right]\frac{di_{j_k}}{dt} + v_j \cdot \frac{\partial L_{j_k}}{\partial x_j} \cdot i_{j_k} \tag{3}$$

$$v_j = \frac{dx_j}{dt} \tag{4}$$

where v_j is the mover speed of the j-th generator and the electromagnetic force can be calculated through the following equation [24],

$$f_j(i_{j_k}, x_j) = \frac{\partial W_c(i_{j_k}, x_j)}{\partial x_j} = \frac{1}{2}\sum_{k=AA'}^{CC'}\left(i_{j_k}{}^2 \cdot \frac{dL_{j_k}}{dx_j}\right) \tag{5}$$

where $W_c(i_{j_k}, x_j)$ is the co-energy. From the above deductions, the complete mathematical model of the ABLSRG can thus be illustrated as,

$$\begin{cases} u_{j_k} = R_{j_k} i_{j_k} + \left[\frac{\partial L_{j_k}}{\partial i_{j_k}} i_{j_k} + L_{j_k}\right]\frac{di_{j_k}}{dt} + v_j \cdot \frac{\partial L_{j_k}}{\partial x_j} \cdot i_{j_k} \\ f_j(i_{j_k}, x_j) = \frac{\partial W_c(i_{j_k}, x_j)}{\partial x_j} = \frac{1}{2}\sum_{k=AA'}^{CC'}\left(i_{j_k}{}^2 \frac{dL_{j_k}}{dx_j}\right) \quad (k = AA', BB', CC', \\ F_j = M\frac{d^2x_j}{dt^2} + Q\frac{dx_j}{dt} + f_j \\ v_j = \frac{dx_j}{dt} \end{cases}$$
$$j = 1, 2) \tag{6}$$

According to the drive topology proposed in [10], each phase applies the typical half-bridge asymmetric drive topology, as shown in Fig. 3. For any phase, the motoring behavior can be depicted in the first equation of (7), when the power transistors are turned on and the diodes are turned off simultaneously; the power generation process can be expressed as the second equation of (7), when the power transistors are turned off and the diodes are turned on, respectively.

$$\begin{cases} U_b - 2U_T = -e + R_{j_k} i_{j_k} \\ e - 2U_D = R' i_{j_k} + R_{j_k} i_{j_k} \end{cases} \tag{7}$$

U_b is the bus voltage, U_T and U_D are the voltage drop of the power transistor (T1–T6) and diode (D1–D6), respectively. e and R' are back electromagnet force and load resistance, respectively.

For any one phase, the changing rate of phase current during motoring can thus be described as,

$$\frac{di_{j_k}}{dx_j} = \frac{U_b - 2U_T}{v_j \cdot L(i_{j_k}, x_j)} - \frac{\frac{\partial \lambda(i_{j_k}, x_j)}{\partial x} \cdot v_j + R_{j_k}}{v_j \cdot L(i_{j_k}, x_j)} \cdot i_{j_k}(x_j) \tag{8}$$

During the power generation period, the changing rate of phase current can be depicted as,

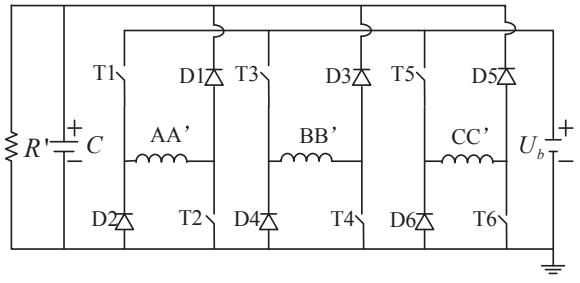

Fig. 3. Drive topology of the ABLSRG.

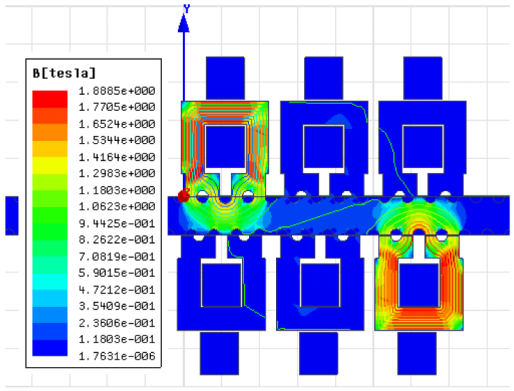

Fig. 4. Electromagnetic characteristics (a) flux contour, (b) mutual inductance and (c) self- inductance.

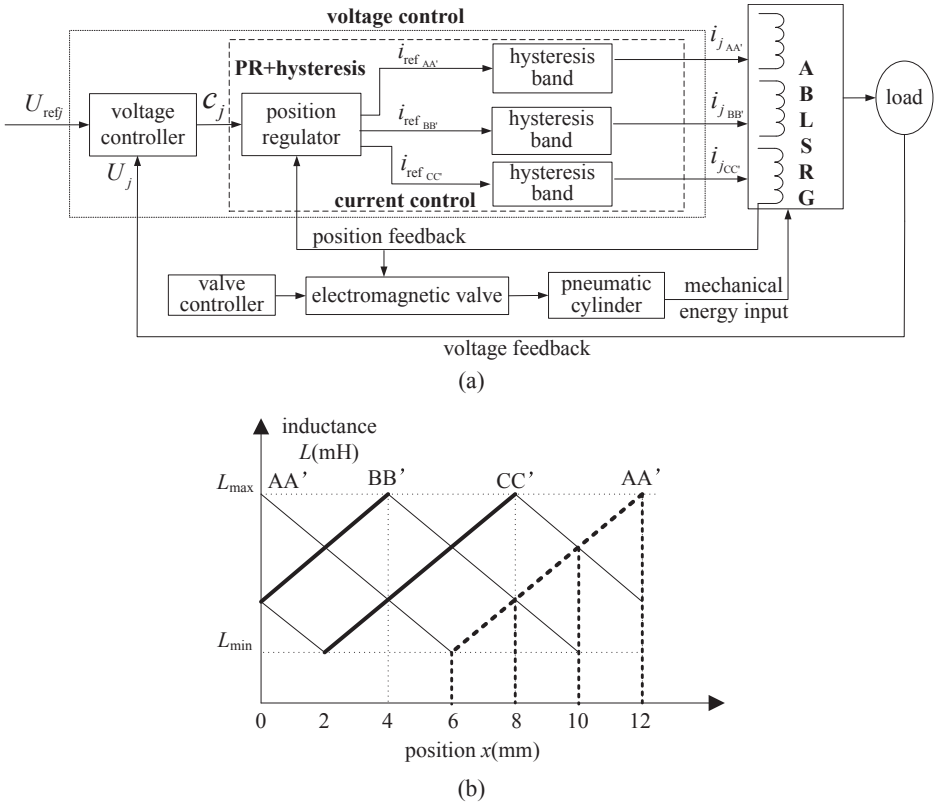

Fig. 5. (a) Voltage control scheme and (b) inductance profiles and excitation scheme.

Table 2
Excitation logic with hysteresis band regulation.

Position	$v \geq 0$		$v < 0$	
	Phase	Value	Phase	Value
0–2 mm	BB′	c_j	AA′,CC′	$i_{jAA'} = c_j/2$ $i_{jCC'} = c_j/2$
2–4 mm	BB′,CC′	$i_{jBB'} = c_j/2$ $i_{jCC'} = c_j/2$	AA′	$i_{jAA'} = c_j$
4–6 mm	CC′	$i_{jCC'} = c_j$	AA′,BB′	$i_{jAA'} = c_j/2$ $i_{jBB'} = c_j/2$
6–8 mm	AA′,CC′	$i_{jAA'} = c_j/2$ $i_{jCC'} = c_j/2$	BB′	$i_{jBB'} = c_j$
8–10 mm	AA′	$i_{jAA'} = c_j$	BB′,CC′	$i_{jBB'} = c_j/2$ $i_{jCC'} = c_j/2$
10–12 mm	AA′,BB′	$i_{jAA'} = c_j/2$ $i_{jBB'} = c_j/2$	CC′	$i_{jCC'} = c_j$

$$\frac{di_{j_k}}{dx_j} = \frac{-U_b - 2U_D}{v_j \cdot L(i_{j_k}, x_j)} - \frac{\frac{\partial \lambda(i_{j_k}, x_j)}{\partial x_j} \cdot v_j + R_{j_k}}{v_j \cdot L(i_{j_k}, x_j)} \cdot i_{j_k}(x_j) \tag{9}$$

Rearranging (3), we have,

$$\begin{aligned} u_{j_k} - R_{j_k} i_{j_k} &= \left[\frac{\partial L_{j_k}}{\partial i_{j_k}} i_{j_k} + L_{j_k} \right] \frac{\partial i_{j_k}}{\partial x_j} \cdot v_j + \frac{\partial L_{j_k}}{\partial x_j} \cdot i_{j_k} \cdot v_j \\ &= \frac{\partial L_{j_k}}{\partial i_{j_k}} \frac{\partial i_{j_k}}{\partial x_j} i_{j_k} \cdot v_j + L_{j_k} \cdot \frac{\partial i_{j_k}}{\partial x_j} \cdot v_j K_{Lj_k} + \frac{\partial L_{j_k}}{\partial x_j} \cdot i_{j_k} \cdot v_j \end{aligned} \tag{10}$$

Since both the phase resistance and the change rate of phase current vs. position can be considered to be small values [14], (10) can be further represented as,

$$u_{j_k} \approx v_j \cdot \frac{\partial L_{j_k}}{\partial x_j} \cdot i_{j_k} \tag{11}$$

Since linear switched reluctance machines have relatively larger air gaps, linear inductance models can be considered [16]. Rewriting (11), we have,

$$u_{j_k} \propto K_{Lj_k} \cdot i_{j_k} \cdot v_j \tag{12}$$

where K_{Lj_k} is the change rate of inductance of the k-th winding for the j-th generator. According to the above deductions, phase voltage can be approximately considered as proportional to v_j, which reflects the energy input capacity from wave. The flux distribution contour can be found in Fig. 4(a). By the finite element method, both mutual inductance and self-inductance values are calculated and plotted for any one phase in Fig. 4(b) and (c), respectively. It can be concluded that any phase is magnetically decoupled and thus can be controlled independently [17].

4. Compensation control design

4.1. Voltage control scheme of single ABLSRG

The voltage control diagram of any generator is shown in Fig. 5. The voltage controller output control command to the position control scheme from the position regulator (PR) module. According to the position feedback signal, the position control block decides which phase (s) should be excited.

On the control of current, the hysteresis band regulator is applied to

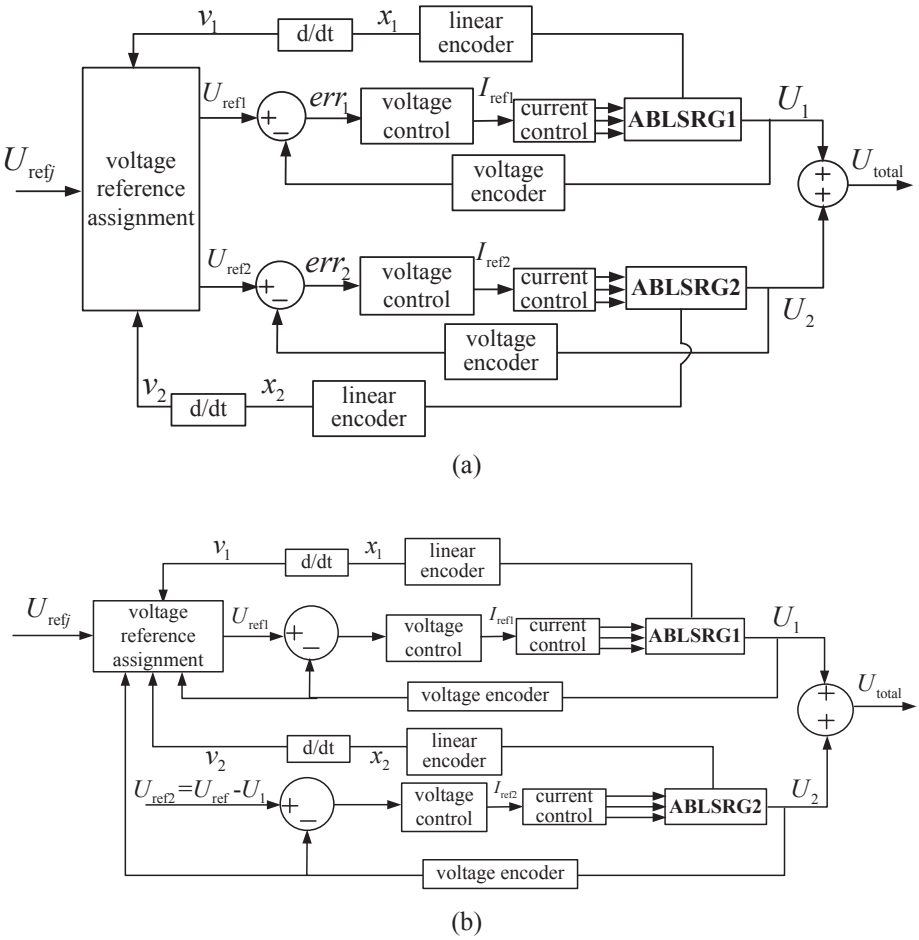

Fig. 6. (a) Independent voltage control and (b) compensation voltage control.

determine the upper C_j and lower band of the current limit. The current control modules regulate the ON and OFF states of the power transistors and the actual voltage is sensed by the voltage transducer and fed back to the voltage controller. Mechanical energy is input by the pneumatic cylinders, regulated by the valve controller and the electromagnetic valves.

Table 2 shows the current excitation logic and current values for each phase i_{jk} (k = AA′, BB′, CC′), according to current position feedback from the hysteresis current regulators. In terms of each phase of the ABLSRG, the MOSFETs are turned on in the inductance rising regions and turned off in the inductance falling regions. The interval for each inductance rising region is 6 mm and it can be evenly divided into three small regions as shown by the dotted line in Fig. 5(b). From Fig. 5(a), c_j is the control output from the voltage controller and the upper limit is set as 4.25 A.

4.2. Independent voltage control

Fig. 6(a) is the independent voltage output control scheme. U_{ref} is the total voltage reference. U_{refj} with j = 1,2, U_1 and U_2, v_1 and v_2 are the voltage reference, actual voltage, and speed of ABLSRG1 and ABLSRG2, respectively. First, the voltage reference assignment mechanism receives the velocity signal of ABLSRG1 and ABLSRG2 to judge if both linear generators have enough power capacity according to the total voltage reference signal U_{ref}. If the speed of both generators are too low (v_1, $v_2 < v' = 0.05$ m/s), it means that the input power capacity is too low and the generators cannot output enough voltage according to U_{ref}. Next, the mechanism divide U_{ref} equally for ABLSRG1 and ABLSRG2 asU_{ref1} and U_{ref2} ($U_{ref} = 2U_{ref1} = 2U_{ref2}$), respectively. Then each linear generator regulates the output voltage signal of U_1 and U_2 in the closed loop manner, as depicted in Fig. 6(a).

It is clear that the total voltage output U_{total} of ABLSRG1 and ABLSRG2 is simply the summation of U_1 and U_2. It can also be concluded that the total output voltage error depends on the performance of each linear generator, since the steady-state error value of the two ABLSRGs is the superposition of the steady-state error values of from two ABLSRGs.

4.3. Compensation voltage control

Fig. 6(b) demonstrates the compensation scheme. Since the speed of the ABLSRG input reflects the wave power capacity, the voltage reference assignment scheme can simply determine the voltage reference signal for ABLSRG1 or ABLSRG2 as,

$$\begin{cases} U_{ref1} = \frac{v_1}{v_1+v_2}\cdot U_{ref} \text{ if } v_1 \geqslant v_2 \\ U_{ref2} = \frac{v_2}{v_1+v_2}\cdot U_{ref} \text{ if } v_1 < v_2 \end{cases} \quad (13)$$

Instead of the difference from $U_{ref}-U_{ref1}$ or $U_{ref}-U_{ref2}$, the voltage reference signal is the difference from the actual output of the other

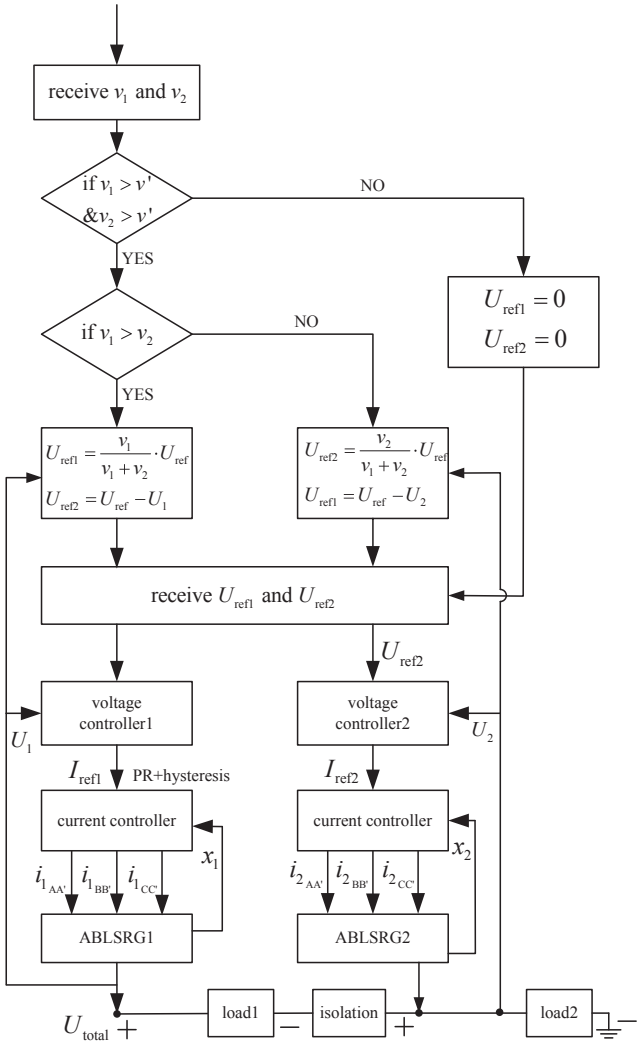

Fig. 7. Compensation control flow chart.

generator. It is clear that such arrangement can compensate the real-time error from ABLSRG1 or ABLSRG2.

From Fig. 6, it is clear that in the independent control scheme, each linear generator controls the voltage output according to its own reference signal (U_{ref1} and U_{ref2}) individually. Total voltage output is the simple summation of U_1 and U_2. However, for the compensation control scheme, voltage reference signal for one ABLSRG is determined by the real time voltage output of U_1 or U_2. Then the voltage reference assignment scheme determines the voltage reference for each generator. Since the two ABLSRGs output voltage complementarily, the precision of the total voltage output can be guaranteed.

The complete control flow chart can thus be illustrated as shown in Fig. 7.

5. Experimentation

5.1. Hardware scheme and experimental setup

Fig. 8(a) is the hardware scheme. Each linear power generation system consists of the controller, the drive circuits, the interface board, the power supplies and the wave power simulation mechanism. The controllers of the two ABLSRGs communicate with serial protocol. The power supplies provide the voltage level of +5 V, ± 15 V, +24 V and +48 V for the integrated chips in the drive circuits of each phase, the wave power control module and the excitation power for the generators. The six phases of the two linear generators applies the asymmetrical half-bridge topologies, and the output current is regulated by the hysteresis controller. The voltage and current protection units protect each phase from over-voltage or over-current. The phase current is detected by the current sensors. Voltage signals from ABLSRG1 and ABLSRG2 are connected in serials after isolation. The power load consists of a power capacity and a resistor connected in parallel. The wave power simulation module consists of the control unit, the electromagnetic valve and the pneumatic cylinder, which is mechanically coupled to the moving platform of the ABLSRG. The cylinder then propels the linear generator and position/velocity is detected by the linear encoder in real-time. The interface boards are responsible for the input of feedback signals and output of control signals, isolated optically.

The drive circuit for each ABLSRG is shown in Fig. 8(b). Since switched reluctance generators require the establishment of the magnetic circuit before generation, the 48 V power supply is employed for excitation. AA′, BB′ and CC′ are connected to the three phases, respectively. Control signals are generated from the controller and transmitted through the octal bus transceiver to the drive circuits of the power transistors. The power transistors apply the Metal-Oxide-Semiconductor Field-Effect Transistors (MOSFETs) IRF740. The load capacitor is charged by the fast switching diodes (MUR1560). Voltage and phase currents are measured by LEM® transducers (LV25-P and LA25-NP).

As shown in Fig. 8(c), the control platforms are two dSPACE® DS1104 real-time processing boards. Control algorithms are developed under *MATLAB/SIMULINK®* environment and downloaded to the digital signal processer of the control boards with control parameters modified online. The voltage and current signals are transmitted through analog-to-digital channels to dSPACE boards. The control signals for each phase are calculated and transmitted to the drive circuits to control the MOSFETs with 5 kHz switching frequency. Fig. 8(d) is the wave power simulation platform. The speed from each cylinder can be regulated by the electromagnetic valves, controlled by the "wave control unit" module. The module consists of a pair of power transistors to control the ON and OFF states of the electromagnetic valve. Meanwhile, since the valves and ABLSRGs are mechanically connected, the speed can also be detected by the linear encoders.

5.2. Experimental results of parameter regulation

Control parameters for each ABLSRG are regulated based on the nominal speed regulated as shown in Fig. 9(a), based on the trial-and-error basis [10]. The simple yet effective proportional-integral-differential (PID) is adopted with the proportional gain (P) to achieve a quick response and improve the control accuracy, while the differential gain D improves the dynamic performance and predicts. The integral gain (I) is responsible for steady-state error reduction. The steady-state voltage profile from Fig. 9(b) demonstrates that the steady-state error voltage can be regulated within ± 0.2 V for each machine. The control parameters are tabulated in Table 3.

If the control parameter such as P or D is changed, the control performance deteriorates and the voltage output profiles can be found in Fig. 9(c) and (d), respectively.

Fig. 9(e) is the phase current waveform, regulated by the upper and lower limit value from the hysteresis band controller. The upper and lower limit of the phase hysteresis band is set as (0.05 A, 0 A). When the

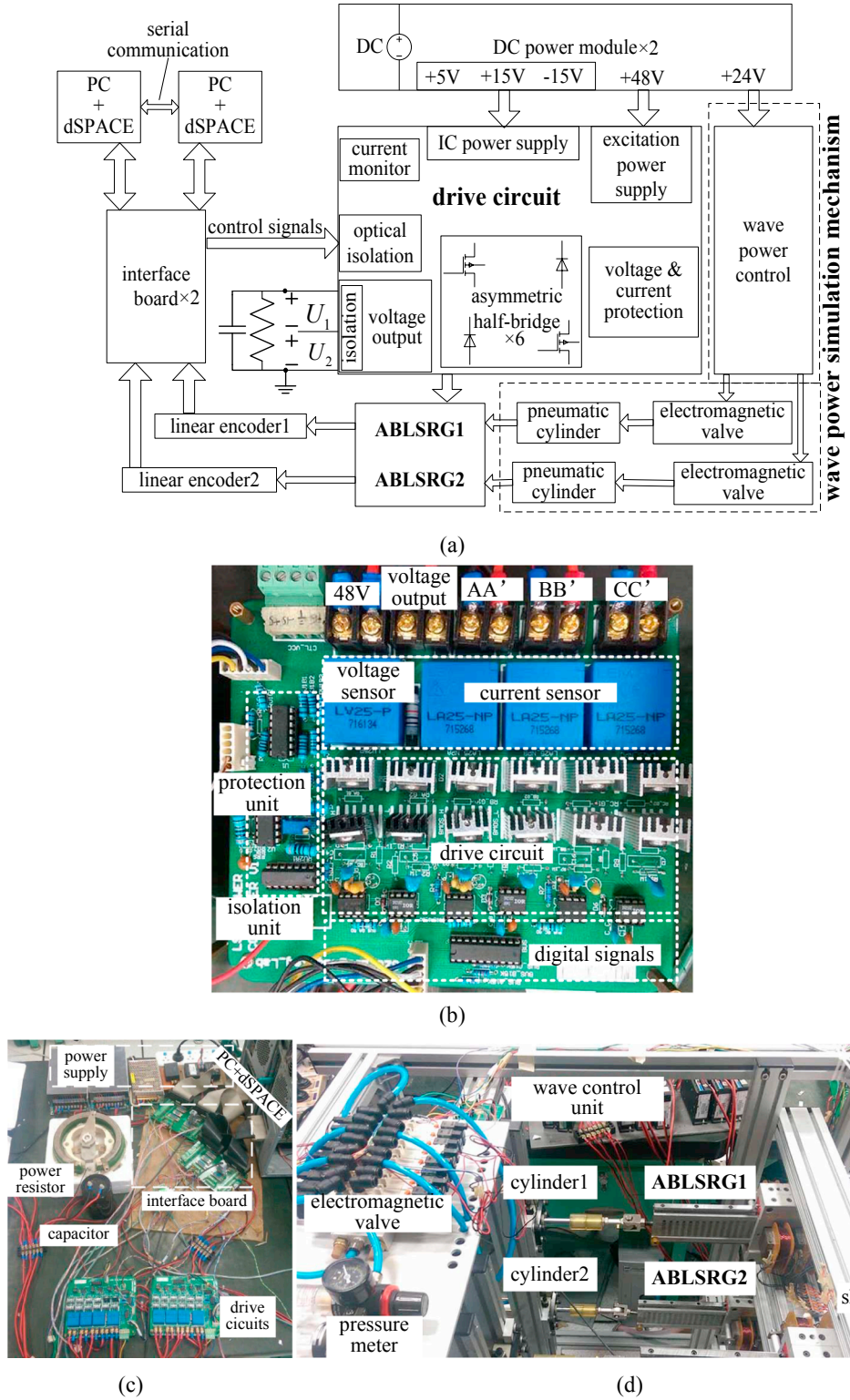

Fig. 8. (a) Hardware diagram, (b) drive circuits, (c) power generation system setup and (d) wave power simulation mechanism.

actual output current exceeds the reference of 1 A and the absolute error is more than 0.05 A, the power transistors will turn off to reduce the actual current output; when the actual output current is less than the reference current and the absolute error is more than 0.05 A, the power transistors will turn on to increase the actual current output.

If the speed waveforms are changed into low speed operation, as illustrated in Fig. 10(a), then the voltage control performance can be found in Fig. 10(b) according to the control parameters regulated from

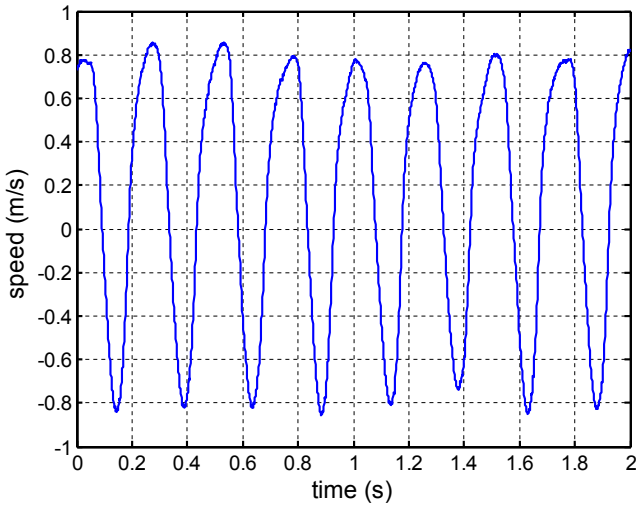

(a)

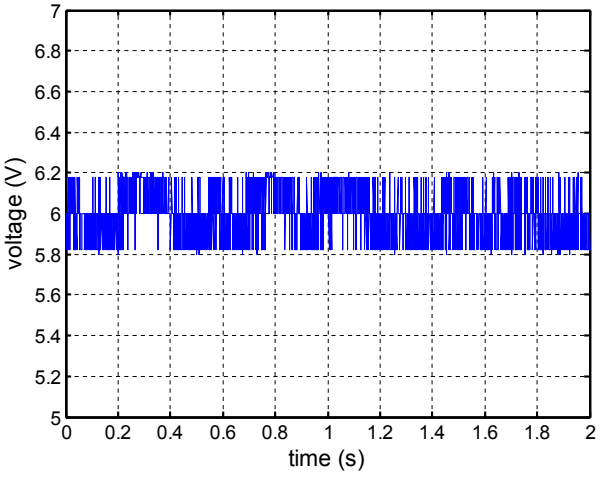

(b)

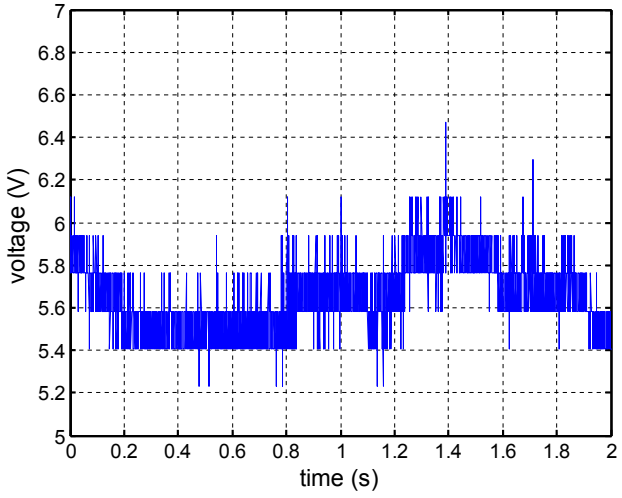

(c)

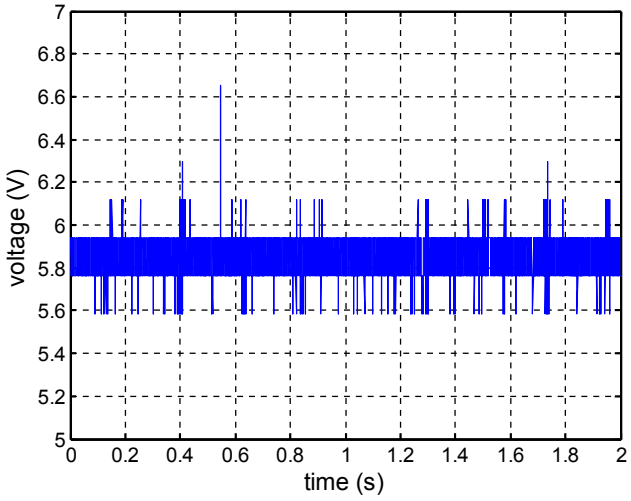

(d)

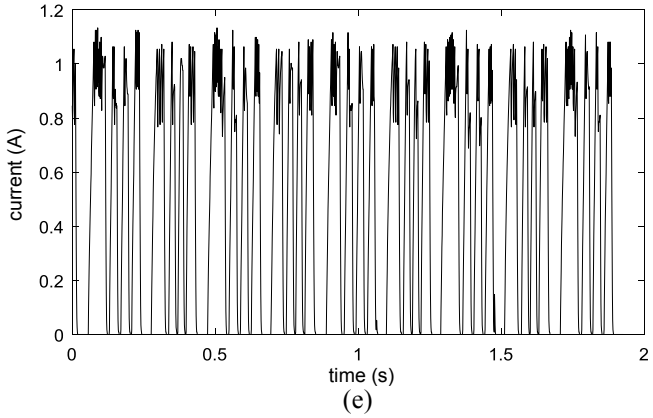

(e)

Fig. 9. (a) Nominal speed waveform, (b) regulated voltage profile, (c) voltage profile with $P = 0.25$, (d) $D = 0.00025$ for single ABLSRG and (e) phase current profiles.

Table 3
Parameters for ABLSRG power generation systems.

Parameter	Value
U_{ref}	12 V
DC bus voltage	48 V
C	100 mF
R'	25 Ω
P	1.5
D	0.002
I	0.0001

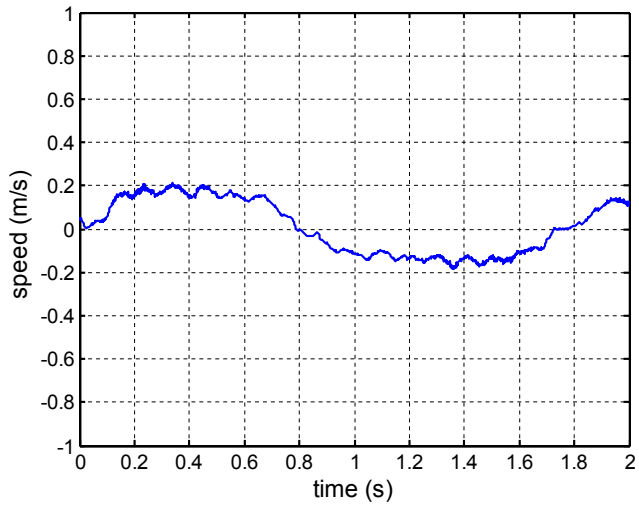

Fig. 10. (a) Low speed waveform and (b) voltage profile at low speed for single ABLSRG.

Table 3. It is clear from the voltage profile that the control precision cannot be guaranteed and there exhibit obvious voltage fluctuations, especially at the intervals (0.3 s, 0.6 s) and (1.3 s, 1.6 s). This is because the generators change the speed direction and the voltage precision cannot be guaranteed under low speed operations, if the control parameters remain unchanged.

5.3. Experimental results of two ABLSRGs

The voltage reference signal is now set as 12 V. The dynamic voltage response profile for each ABLSRG can be found in Fig. 11(a). Due to the capacity of the generator, the voltage waveform drops sharply as the reference level exceeds 8 V. Fig. 11(b) shows the voltage profile from the control algorithm according to Fig. 6(a). The voltage waveform fluctuates from 11.5 V to 12.4 V. Since the voltage is obtained from each ABLSRG independently, the steady-state precision is almost equal to the summation from each generator. If P is changed, the total output voltage level decreases because the system gains for each generation system are decreased. In addition, the control performance deteriorates with maximum fluctuation falling into 11–12.4 V, as shown in Fig. 11(c). The decrease of D also influences the performance of output voltage. From Fig. 11(d), the fluctuation range is 11.3–12.5 V. Meanwhile, the entire response profile moves downward and most of the voltage output values are less than 12 V. Therefore, the independent voltage control method is no longer able to adapt to the variations of control parameters.

The voltage response waveforms under the speed profile depicted in Fig. 10(a) can be found in Fig. 11(e). Under low speed operations, there exhibit dominant voltage fluctuations, especially at the intervals of (0.3 s 0.6 s) and (1.3 s 1.6 s) as the machines experience direction change. Therefore, the independent control scheme is not capable to guarantee the total voltage output.

The voltage response waveforms under the compensation control scheme can be found in Fig. 12(a). It can be seen that the total voltage level falls into 11.8–12.2 V and the steady-state of ± 0.2 V can be achieved. If the gains of P and D are changed, the voltage profiles can be regulated within the range of 11.75–12.23 V and the commutation does not affect the performance, as shown in Fig. 12(b) and (c). From Fig. 12(d), under low speed operations, there are small variations of the voltage profile and the control precision from the steady states can be obtained. The steady-state error can be maintained as 11.79–12.22 V. The experimental results demonstrate that the proposed compensation control scheme has certain robustness and the steady-state error values can be guaranteed.

6. Conclusion

This paper discusses about the compensation power generation control of two ABLSRGs. The capacity one single generator is limited and the independent power generation cannot guarantee a precise voltage output. The simple yet effective compensation generation scheme increases the power capacity, as well as achieves the steady-state precision of voltage output. Experimental results demonstrate that in the condition of control parameter variations, the proposed compensation scheme has certain robustness and the steady-state error values are falling into 11.75–12.23 V. It also shows that the proposed control scheme adapts to the conditions of speed variations, while the independent power generation control exhibits large voltage fluctuations. It is suggested that the proposed compensation method be applied for the coordination power generation of more ABLSRGs.

The wave behaviors are simulated by pneumatic cylinders, regulated by the electromagnetic valves and valve controllers. Therefore the input is not ideally sinusoidal and the input speed cannot be controlled precisely. However, the proposed complementary voltage control scheme is able to counteract such influence of the imperfect wave simulation and achieve a precise voltage control results. Future work will focus on the propulsion by direct drive linear electric machines as mechanical input for a precise wave input simulation, for example, linear permanent magnet synchronous motors.

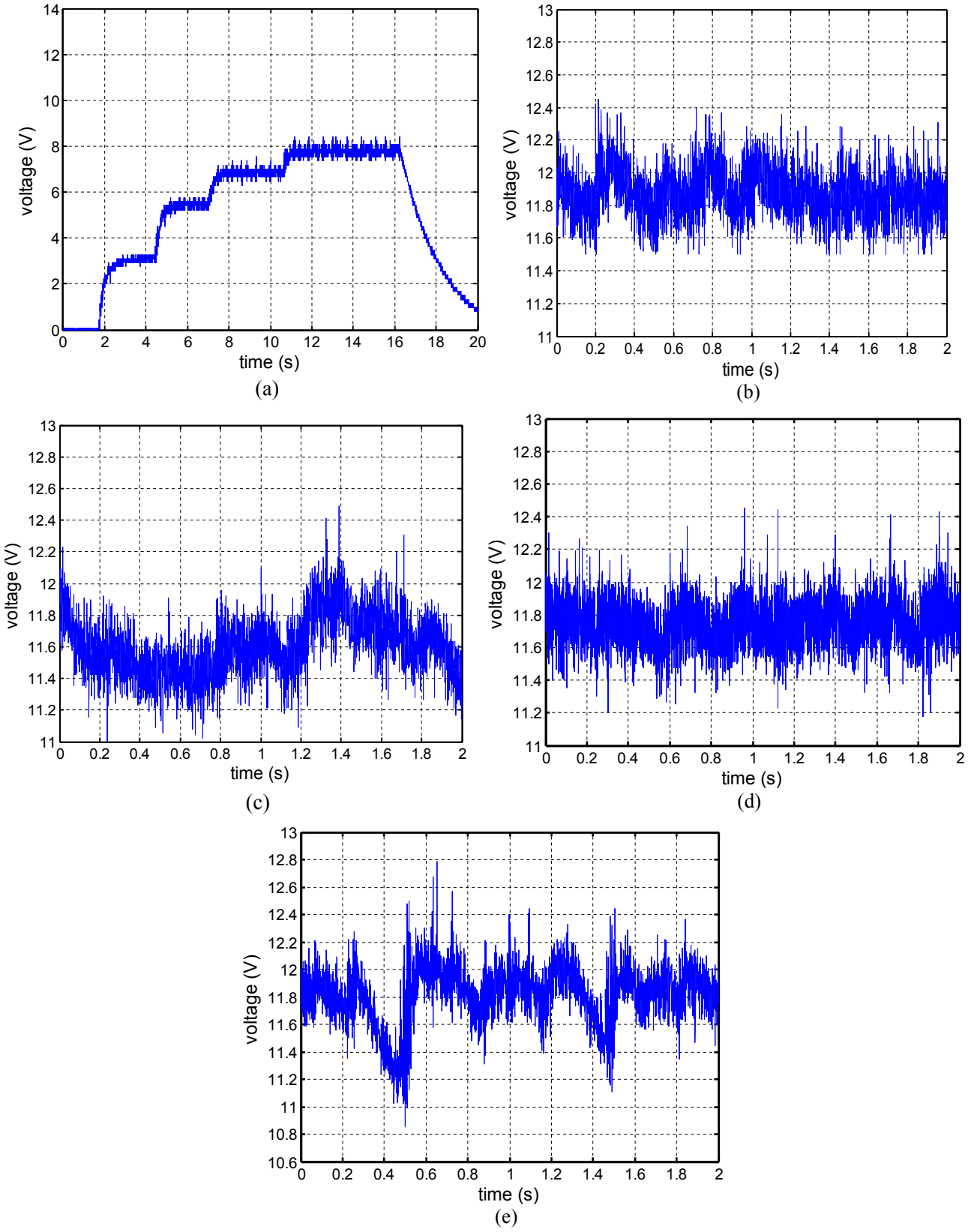

Fig. 11. (a) Voltage response of 12 V of single generator, (b) voltage profile under independent control, (c) response as $P = 0.25$, (d) response as $D = 0.00025$ and (e) voltage profile under low speed.

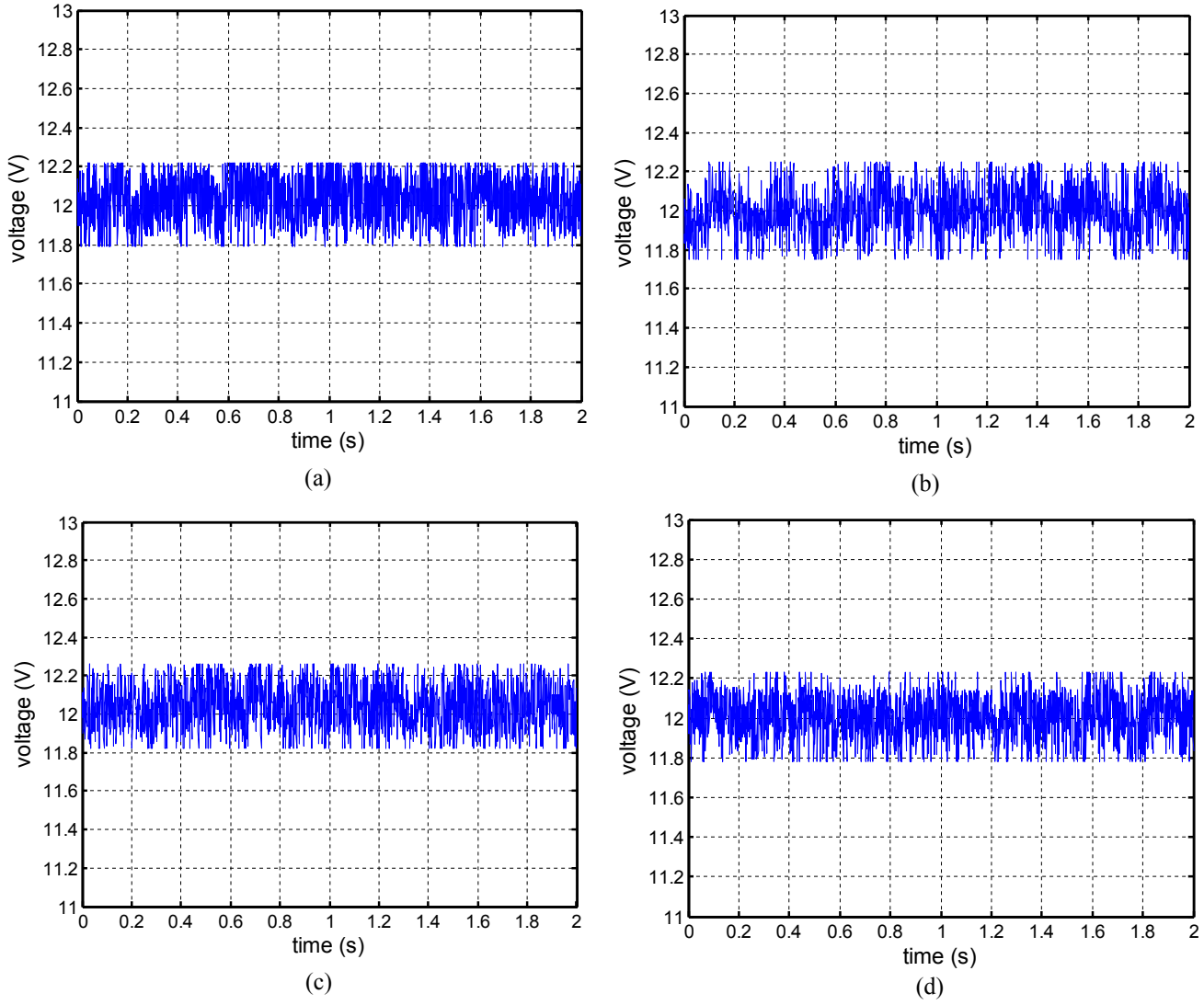

Fig. 12. (a) Voltage profile under compensation control, (b) response as $P = 0.25$, (c) response as $D = 0.00025$ and (d) voltage profile under low speed.

Acknowledgment

This work was supported by the National Natural Science Foundation of China under Grant 51477103 and 61873170. The authors would also like to thank the Guangdong Natural Science Foundation under Grant 2015A010106017 and 2016KZDXM007.

Appendix A. Supplementary material

Supplementary data to this article can be found online at https://doi.org/10.1016/j.ijepes.2018.09.023.

References

[1] Castro-Santos Laura, Garcia Geuffer Prado, Estanqueiro Ana, Justino Paulo APS. The levelized cost of energy (LCOE) of wave energy using GIS based analysis: the case study of Portugal. Int J Electr Power Energy Syst 2015;65(February):21–5.
[2] Falnes J. A review of wave-energy extraction. Mar Struct 2007;20(September):185–201.
[3] Scruggs J, Jacob P. Harvesting ocean wave energy. Science 2009;323:1176–8.
[4] Liermann Matthias, Samhoury Omar, Atshan Samer. Energy efficiency of pneumatic power take-off for wave energy converter. Int J Mar Energy 2016;13(April):62–79.
[5] Lettenmaier Terry, von Jouanne Annette, Brekken Ted. A new maximum power point tracking algorithm for ocean wave energy converters. Int J Mar Energy 2017;17(April):40–55.
[6] Wahyudie A, Jama MA, Susilo TB, Saeed O, Nandar CSA, Harib K. Simple bottom-up hierarchical control strategy for heaving wave energy converters. Int J Electr Power Energy Syst 2017;87(May):211–21.
[7] Jones WD. Update—ocean power catches a wave. IEEE Spectr 2008;45(7):14–27.
[8] Pan JF, Zou Yu, Cheung Norbert, Cao Guangzhong. The direct-drive sensorless generation system for wave energy utilization. Int J Electr Power Energy Syst 2014;62(November):29–37.
[9] Widyan Mohammad S, Hanitsch Rolf E. High-power density radial-flux permanent-magnet sinusoidal three-phase three-slot four-pole electrical generator. Int J Electr Power Energy Syst 2012;43(1):1221–7.
[10] Pan JF, Zou Y, Cheung N, Cao GZ. On the voltage ripple reduction control of the linear switched reluctance generator for wave energy utilization. IEEE Trans Power Electron 2014;29(10):5298–307.
[11] Dang TT, Ruellan M, Prévond L, Ben Ahmed H, Multon B. Sizing optimization of tubular linear induction generator and its possible application in high acceleration free-piston Stirling microcogeneration. IEEE Trans Ind Appl 2015;51(5):3716–33.
[12] Faiz J, Azami A, Keyhani A, Proca A. Closed-loop control stability for permanent magnet synchronous motor. Int J Electr Power Energy Syst 1997;19(5):331–7.
[13] Errami Youssef, Ouassaid Mohammed, Maaroufi Mohamed. A performance comparison of a nonlinear and a linear control for grid connected PMSG wind energy conversion system. Int J Electr Power Energy Syst 2015;68(June):180–94.
[14] Miller TJE. Switched reluctance motors and their control. USA: Oxford University Press; 1993. p. 25–8.
[15] Yassami Hossein, Bayat Farhad, Jalilvand Abolfazl, Rabiee Abbas. Coordinated voltage control of wind-penetrated power systems via state feedback control. Int J Electr Power Energy Syst 2017;93(December):384–94.
[16] Pan J, Zou Y, Cao G. Investigation of a low-power, double-sided switched reluctance generator for wave energy conversion. IET Renew Power Gener 2013;7(2):98–109.
[17] Pan JF, Zou Y, Cao G. An asymmetric linear switched reluctance motor. IEEE Trans

Energy Convers 2013;28(2):444–51.
[18] Zulkifli SA, Karsiti MN, Aziz Abd Rashid Abd. 2008 IEEE 2nd international power and energy conference, Johor Bahru. 2008. p. 1086–91.
[19] Chen H, Wang Xing, Gu JJ. Sliding mode control of Switched Reluctance linear generator system. 2009 International conference on networking, sensing and control, Okayama. 2009. p. 779–82.
[20] Abe FY, Chabu IE, Matakas L. DC link voltage control for direct drive linear wave energy converter. 2017 IEEE 8th international symposium on power electronics for distributed generation systems (PEDG), Florianopolis. 2017. p. 1–8.
[21] Ran L, Mueller MA, Ng C, Tavner PJ, Zhao H, Baker NJ, et al. Power conversion and control for a linear direct drive permanent magnet generator for wave energy. IET Renew Power Gener 2011;5(1):1–9.
[22] Ding Wen, Liu Ling, Yanfang Hu, Liu Yunpeng. Modular switched reluctance machine with E-core stators and segmental rotors for high reliability applications. Int J Electr Power Energy Syst 2014;62(November):496–506.
[23] Daryabeigi Ehsan, Dehkordi Behzad Mirzaeian. Smart bacterial foraging algorithm based controller for speed control of switched reluctance motor drives. Int J Electr Power Energy Syst 2014;62(November):364–73.
[24] Kalaivani L, Subburaj P, Iruthayarajan M Willjuice. Speed control of switched reluctance motor with torque ripple reduction using non-dominated sorting genetic algorithm. Int J Electr Power Energy Syst 2013;53(December):69–77.